Lüders, V. (2017): Contribution of infrared microscopy to studies of fluid inclusions hosted in some opaque ore minerals: possibilities, limitations, and perspectives. - *Mineralium Deposita*, *52*, 5, pp. 663—673.

DOI: http://doi.org/10.1007/s00126-016-0694-4

Contribution of infrared microscopy to studies of fluid inclusions hosted in some opaque ore minerals: Possibilities, limitations and perspectives.

Abstract During the past two decades several studies of fluid inclusions hosted in some opaque ore minerals using nearinfrared microscopy have been performed. Results indicated that this method can be applied to several sulfidic ores and metal oxides depending on their electronic band structures and infrared-active vibration modes. Infrared transmittance of individual ore minerals can be best characterized using Fourier transform infrared spectroscopy. Iinfrared microscopic observations are limited to the near-infrared region to about 2.3 μm depending on the IR sensitivity of the IR camera. The trace element content in ore minerals can be another limiting factor for optical observations in near-infrared light. Still, IR transmittance gradually decreases upon heating caused by shifting of IR absorption edges for higher wavelengths. Possibilities and limitations studying fluid inclusions hosted in opaque minerals by near-infrared light microthermometry and laser ablation-inductively coupled plasma- mass spectrometry (LA-ICP-MS) are discussed.

Introduction

Fluid inclusions hosted in minerals yield important information in ore deposit research because they are faithful recorders of *PVTX* constrains of ore-forming fluids. Fluid inclusions data may provide important information on ore genesis and may are useful tools for prospection and exploration, i.e., fluid inclusion studies may assist in determining and delineating individual mineral deposits and mineral provinces (e.g. Moncada et al. 2012; Bodnar et al. 2014).

Fluid inclusions hosted in minerals are commonly studied under visible light using microthermometry and sophisticated instrumentation such as laser-Raman spectroscopy, LA-ICP-MS, etc. In ore deposit research the study of fluid inclusions in gangue minerals such as quartz, carbonates, fluorite, etc. which are transparent for visible light is well-established. The data obtained are inferred to decipher the *PVTX* properties during ore formation under the assumption of co-genetic deposition of mineral associations of sulfides and/or metal oxides and gangue minerals in ore deposits from the same fluid. Roedder and Bodnar (1997) pointed out that almost all information about temperature, composition, density, and pressure of ore-

29 forming fluids in fossil hydrothermal ore deposits are derived from fluid inclusionstudies Studies of fluid
30 inclusions hosted in bright sphalerite and associated gangue minerals have shown that locally ore and gangue
31 minerals may contain fluids of different composition (e.g. Woods et al. 1982; Behr et al. 1987; Wilkinson
32 2001; Shimizu and Masahiro 2003) and caution must be paid when solely using fluid inclusion data of
33 gangue mineral-hosted fluid inclusions to infer the *PVTX* constrains of ore formation.
34 Most of the economically important ore minerals are opaque in transmitted light and therefore excluded for
35 traditional microthermometric investigations. Several studies, however, have shown that some ore minerals
36 are transparent in the near infrared region (e.g. Campbell and Robinson-Cook 1987; Campbell and Panter
37 1990; Richards and Kerrich 1993; Mancano and Campbell 1995; Lüders 1996; Lüders and Ziemann 1999;
38 Lüders et al. 1999; Bailly et al. 1999; Kouzmanov et al. 2002; Rosière and Rios 2004; Lüders et al. 2005;
39 Zhu et al. 2013; Ni et al. 2015). Thus infrared microscopy provides a means to study fluid inclusions hosted
40 in opaque ore minerals such as metal oxides, pyrite, wurtzite, stibnite, some sulfosalts and others in the near
41 infrared region.
42 This paper aims at the the possibilities and limitations of infrared microscopy applied to fluid inclusion
43 studies in opaque ore minerals particularly in combination with dating of fluid events or LA-ICP-MS
44 analysis of fluid inclusions hosted in ore minerals.
45
46 **Infrared transmittance of ore minerals**
47
48 The infrared transmittance of minerals depends on their individual band structures and infrared-active
49 vibration modes (e.g. Hunt et al. 1971a,b; Shuey 1975; Boldish and White 1998). Many ore minerals are
50 natural extrinsic (impurity) semiconductors and differ from conductors such as Au, Ag, and Cu by their non-
51 metallic bonds.
52 The band theory of solids (or energy band model) implies that in semiconductors the valence band (occupied
53 with electrons) is separated from the conduction band (almost unoccupied with electrons) by a band gap (Fig.
54 1a). The minimum energy that is required to excite an electron to move from the valence band to the
55 conduction band is called band gap energy (*Eg* in Fig 1a). The band gap energy is given in eV and is
56 different for individual ore minerals (Shuey 1975; Boldish and White 1998). Minerals such as quartz,

fluorite, carbonates and even some ore minerals (e.g. Fe-poor sphalerite, proustite, cinnarbar) having band gap energies greater than 1.7 eV are transparent for visible light (1.7 to 3.3 eV). In contrast, the majority of ore minerals have band gap energies less than 1.7 eV and photons with equal or greater energy will be absorbed. Infrared light covers a broad range of photon energy from 1.7 eV to 0.00124 eV corresponding to a wavelength range $\lambda = 0.73$ to 1000 μm.

The inverse relationship between the photon energy and the wavelength of light is given equation:

$$E\ (eV) = {}^{1.2398}/_{\lambda\ (\mu m)} \qquad (1)$$

Thus photons with lower energy than the band gap energy only weakly interact with the surface and will pass. For example, galena which has band gap energy of 0.37 eV (Schoolar and Dixon 1965) absorbs all near infrared-light with wavelength $\lambda < 3.35$ μm, but will be transparent for photons having lower energy than 0.37 eV, i.e., galena is transparent at wavelength $\lambda > 3.35$ μm. This is illustrated in Fig. 2 showing the Fourier transformation infrared (FT-IR) spectra of galena from various occurrences in the spectral range $\lambda =$ 1 to 4 μm (near infrared to beginning of mid infrared region). In contrast, stibnite with band gap energy of 1.72 eV (Efstathiou and Levin 1968) is always transparent for near-infrared light in the spectral range $\lambda = 1$ and 2.5 μm (Fig. 3). The same holds true for studied samples of enargite and bournonite (Fig. 3).

The infrared transmittance of minerals strongly depends on the crystal structure andchemistry, which both define the band gap energies. However, also impurities within the crystal lattice may diminish the band gap energy and cause a decrease in infrared-light transmission.

In semiconductors the number of free electrons is less than that in conductors. The valence electrons are arranged in couples in the form of electron bridges between the atoms. These electron bridges can be broken by e.g. thermal excitation or absorption of light (photon energy) and excited electrons can move from the valence band to the conduction band due to their higher changed energy state. Semiconductors having the same number of electrons and holes are called intrinsic semiconductors. Doping of a semiconductor by impurity atoms of a different element with either higher or lower numbers of valence electrons into the crystal lattice of a semiconductor causes a change of the charge carrier density. Impurity semiconductors

84 (e.g. natural semiconducting ore minerals) are either n-type or p-type semiconductorswhen there is a
85 transport of negative charge in the form of electrons or defect electrons (positive holes), respectively for
86 details see e.g. Shuey, 1975). The conductivity of both n-type and p-type semiconductors is enhanced
87 compared to that of intrinsic semiconductors (Fig. 1b and c). In both n-type and p-type semiconductors the
88 concentration of valence electrons or holes, respectively, is higher than those of an intrinsic semiconductor.
89 The surplus valence electrons of the impurity atoms in an n-type semiconductor are only weakly bound and
90 the energy states lie close to the valence band in a so-called donor level (Fig. 1b). Thus only little energy
91 (less than the band gap energy) is needed to excite electrons to move from the donor level to the conduction
92 band resulting in a high conductivity and thus in absorption of even lower energy photons. In contrast, p-type
93 semiconductors have a shortage of electrons and thus the donor level lies closer to the valence band (Fig. 1c).
94 Only little energy is required to donate electrons from the valence band to the impurity atoms, thus resulting
95 in an increased number of mobile defect electrons (holes) in the valence band.
96
97 **Semiconducting ore minerals**
98
99 Many sulfides as well as some metal oxides (e.g. hematite, Mn-oxides, wolframite or Nb-Ta oxides) are
100 good semiconductors (Hunt et al. 1971a,b, Shuey 1975). However, the band gap energies of individual
101 sulfides and oxides are highly variable. For example, Fe-poor sphalerite has band gap energy of nearly 4 eV
102 (Shuey, 1975) and thus is nearly an isolator whereas pyrrhotite has band gap energy of nearly 0 eV and is
103 almost a conductor. Other sulfides have variable but almost low band energies (Shuey 1975): e.g.
104 arsenopyrite 0.2 eV, galena 0.37 eV, pyrite 0.9 eV, chalcopyrite 1.1 eV. Depending on doping with impurity
105 atoms (electron donators or electron acceptors), natural semiconductors e.g. galena, arsenopyrite,
106 molybdenite or pyrite can be either n-type or p-type semiconductors (Shuey 1975). Common impurities for
107 example in pyrite are Co, Ni, Zn, Cu and As (Fleischer 1955, Kulis 1999; Kouzmanov et al. 2010). Hawley
108 (1952), Fischer and Hiller (1956) and Favorov et al. (1972) have studied the semi conductive properties of
109 natural pyrites and showed that pyrites with high Co and Ni or high Cu content are n-type semiconductors
110 whereas As-rich pyrites are p-type semiconductors. Furthermore, Karasev et al. (1972) suggested that pyrites
111 from high-temperature hydrothermal veins and pegmatites in the absence of arsenopyrite tend to be n-type

112 semiconductors, whereas sedimentary pyrites in the absence of Cu minerals are commonly p-type
113 semiconductors. FT-IR transmission spectra of hydrothermal pyrites display sharp adsorption edges
114 (hydrothermal pyrites; n-type) whereas sedimentary pyrites show either FT-IR spectra with poor or even no
115 IR transmittance (Lüders and Ziemann 1999, Lindaas et al. 2002, Kouzmanov et al. 2002).
116 Sphalerite provides an extreme example of how impurities can determine the band gap energy . As
117 mentioned above, sphalerite has wide range of band gap energies up to about 4 eV. However, Keys et al.
118 (1968) studied a natural sphalerite sample with high Fe content of 12.4 wt. % and measured band gap energy
119 of 0.5 eV and attributed this to impurity-induced conductivity. Fig. 4 shows selected FT-IR spectra of iron-
120 poor and iron-rich sphalerite samples from hydrothermal mineralization. The iron-poor sphalerite sample
121 from Neudorf is also transparent for visible light and shows constant IR light transmittance in the wavelength
122 range between λ = 0.9 and 1.9 μm. At higher wavelengths the IR transmittance of the Neudorf sample (and
123 all other samples) decreases and the sample becomes opaque for near IR light at about 2.4 μm (Fig. 4). The
124 infrared adsorption edges of iron-rich sphalerites and wurtzites are typically shifted towards higher
125 wavelengths and fluid inclusions in iron-rich sphalerite can only be observed using near infrared light
126 microscopy (Fig. 4). The FT-IR spectra of studied sphalerite samples from high-T (280-340°C) hydrothermal
127 mineralization (Freiberg; Lavrion) differ from the spectra of sphalerites from magmatic systems (N´Fiji
128 Basin; Zinnwald). So far, no statement can be made whether the FT-IR spectra of sphalerite yield
129 information about the origin of the ore-forming fluids due the limited number of studied samples.
130 Besides impurities, the chemical composition may have a significant impact on the infrared transmittance of
131 semiconducting sulfide minerals (Boldish and White 1998). For example, fahlores widely occur in
132 hydrothermal mineralization and are complex sulfosalts which form solid solution series of the tetrahedrite
133 ($Cu_{10}(Fe,Zn)_2Sb_4S_{13}$)-tennantite ($Cu_{10}(Fe,Zn)_2As_4S_{13}$) group between both endmembers. Considerable
134 amounts of the Cu can also be replaced by other element such as Ag in freibergite
135 ($((Ag,Cu))_6(Ag,Cu)_4(Fe,Zn)_2Sb_4S_{12-13}$), Hg in schwazite ($((Cu,Hg)_{12}Sb_4S_{13}$) or Te in Goldfieldite ($Cu_{10-12}(Te,Sb,As,Bi)_{4-6}S_{13}$). Only little is known about the semiconductive properties of fahlores. The band gap
137 energy is assumed to be not greater than 1 mV (Wernik and Beson 1957). Cu, Ag members are assumed to
138 be p-type semiconductors whereas Fe-rich members are more likely n-type semiconductors (Telkes 1950).
139 Table 1 shows the results of microprobe analyses of 13 fahlore samples from different occurrences. All

140 samples have been inspected under the IR microscope for optical features and it turned out that Sb-rich
141 fahlore (tetrahedrite) shows good IR transparency whereas the IR transmittance decreases with increasing As
142 content (Table 1). As-rich fahlores (tennantite) are even opaque under the IR microscope. However, also
143 increased Hg and or Ag content have a strong impact on the visible IR transmittance of the studied samples
144 Table 1). This is also reflected by the FT-IR spectra of some of the studied samples (Fig. 5). The tetrahedrite
145 sample from Clausthal (Harz Mts., Germany) with low As concentration shows very good IR transmittance
146 in the near infrared region that decreases rapidly to ca. 1.7 to 1.8 µm (Fig. 5). The IR transmittance of the
147 As-bearing tetrahedrite sample from Silverton (Colorado, USA) is considerably lower and there is even no
148 IR transmittance in a studied tennantite endmember sample from Redruth (Cornwall, UK) in the near
149 infrared region.
150
151 **Infrared microscopes and cameras**
152
153 Microscopic infrared images of fluid inclusions in opaque minerals that are transparent for near infrared light
154 can be obtained in two different ways. The Research Devices Model F infrared microscope which is
155 described in detail by Campbell (1991) was used in previous infrared microthermometric studies (Campbell
156 and Robinson-Cook 1987). In this microscope, a visible image is projected via an infrared sensitive plate on
157 to a fluorescent screen. The Research Devices Model F infrared microscope allows observations in the near-
158 infrared light region in the wavelength range between λ = 800 - 1200 nm (= 0.8 – 1.2 µm) with a maximum
159 magnification of 400 X.
160 Other microscopes such as the obsolescent Olympus BHSM-IR, the modified Olympus BX 53, or Leica
161 DMRM use an infrared-sensitive TV camera to display the infrared image to a monitor screen. The optics of
162 these microscopes are specially coated for IR application and IR objectives with consistent IR transmittance
163 in the spectral range λ = 0.8 to 3 µm are available. Some new microscopes on the market are suitable for
164 applications in visible light and in the near IR to wavelengths up to about 1 µm. The transformation of the IR
165 image to a monitor screen can done either be by digital IR-sensitive cameras or by special analog IR cameras
166 with extremely sensitive IR tubes. Today, microscopic observations in the near IR are limited to the spectral

range λ = 0.78 to 2.3 µm and minerals which show IR transmittance above 2.3 µm (for example galena, Fig. 2) are excluded for microthermometric investigations.

The resolution of simple IR sensitive CCD cameras is usually not better than 1 µm (Fig. 6). These cameras are suitable to observe fluid inclusions in semiconducting ore minerals with band gap energies greater than 1 eV such as e.g. enargite, bournonite, wolframite (Fig. 7) and, under best circumstances hematite (Fig. 8). Fluid inclusions hosted in semiconducting sulfides with lower band gap energies (e.g. pyrite) can be studied only with highly sensitive IR cameras (Fig. 9). InGaAs cameras which are new on the market show highly constant sensitivity in the near infrared region up to 1.8 µm (Fig. 6). At the moment, the highest resolution of about 2.3 µm can be obtained when using a Dage-MTI camera with a Hamamatsu N2006-06 selected IR tube. However, the sensitivity of such IR tubes is much lower compared to that of InGaAs cameras in the spectral range λ = 1 to 1.8 µm and decreases continuously towards higher wavelengths (Fig. 6).

Optical observations in near infrared light

A very important aspect that has a huge impact on the IR transparency of ore minerals is the thickness of the polished sections. Kulis (1999) studied the relationship between the temperature of opacity (i.e., the temperature at which the pyrite samples become opaque on the monitor screen upon heating) and the thickness of the polished pyrite sections. His studies show an approximately exponential relationship between temperature of opacity and thickness of the pyrite sections assuming similar adsorption coefficient of the studied sample.

Although several ore minerals show good transmittance for near IR light, fluid inclusions hosted therein may show only poor or even no transparency. Richards and Kerrich (1993) were the first to observe dark fluid inclusions in pyrite samples and attributed the opacity of the pyrite-hosted inclusions to an intense refraction of IR light resulting from the high refraction contrast between pyrite and aqueous phase fluids. Kulis (1999) concluded that especially fluid inclusions hosted in pyrite that are tilted relative to the surface of the polished thick section often appear opaque due to the high IR refraction index of pyrite compared to that of water. However, it is noteworthy that opaque inclusions can be observed also in other ore minerals such as e.g.

chalcopyrite, sphalerite, sulfosalts or wolframite. Therefore, the phenomenon of high IR light refraction between ore minerals and water-bearing fluid inclusions hosted therein is not restricted to pyrite.

Technical details for studies of fluid inclusions in near-infrared light

Transmitted light microscopes are equipped with an IR filter which is placed in the pathway of the light in order to prevent heat being produced by infrared radiation from the sample. In contrast, microscopes being suitable for observations in the near-infrared region are equipped with special IR band pass filters that allow infrared light to pass through the microscope.

Fluid inclusion studies using infrared microscopy applied to fluid inclusions hosted in opaque ore minerals gave rise to debate whether or not infrared radiation falsifies the results of microthermometry due to enhanced heat production. Moritz (2006) studied enargite-hosted fluid inclusions using an infrared microscope equipped with a USGS gas-flow heating/freezing stage. When using different IR cameras; i.e., a Hamamatsu IR tube camera that requires high IR light intensity as well as a CCD IR camera (low IR light intensity) Moritz (2006) observed a significant difference of ice melting temperatures, which he attributed to to the effect of light intensity on phase transitions in fluid inclusions. He concluded that measured final ice melting temperatures decrease considerably with increasing intensity of light and yield wrong salinities.

Other studies using a Hamamatsu IR tube camera and the USGS gas-flow heating/freezing stage show constant temperatures for ice melting and homogenization of pyrite-hosted fluid inclusions even when using very high light intensity (e.g. Lüders and Ziemann 1999; Kouzmanov et al. 2002). Lindaas et al. (2002) tested the effect of infrared radiation of the sample and the thermocouple of the USGS gas-flow heating/freezing stage and found a standard deviation of the final melting temperatures of ± 0.4°C for five times repeated measurements of the same inclusion using infrared light. When using a Linkam heating/freezing stage and infrared light the standard deviation was even less (± 0.1°C). Pflugbeil (1995) conducted multiple measurements for calibrating the thermocouple of the USGS stage under transmitted and infrared light using synthetic fluid inclusion standards (Syn Flinc) of known melting and homogenization temperatures as well as fluid inclusions hosted in natural samples (quartz, sphalerite). During the measurements care was taken that the thermocouple was placed outside the light beam. In this way, the

222 correlation of measurements in transmitted and transmitted near-infrared light appeared to be very consistent
223 (Fig 10).
224 When using a USGS gas-flow heating/freezing stage it is important to adjusting the aperture diaphragm
225 down in a way so that the thermocouple which fixes the sample is not positioned within the path of the light
226 beam. When using a Linkam stage the effect of heating is negligible as long as the diaphragm is cut down
227 enough to prevent heating of the silver block.
228 By the use of CCD or InGaAs IR cameras the light intensity being necessary for fluid inclusion phase
229 transition observations is very low and temperature deviations due to IR heating can be ruled out.
230 As pointed out above, many ore minerals are impurity semiconductors. The intrinsic conduction of
231 semiconductors increases with increasing temperature and shifts the infrared absorption edge towards higher
232 wavelengths (e.g. Seehra and Seehra 1979; Lüders and Ziemann 1999; Lindaas et al. 2002). The shift of the
233 IR absorption edges of semiconducting ore minerals has a huge impact for observing of phase transitions of
234 fluid inclusions during heating runs. Campbell et al. (1988) observed that wolframite samples from the
235 Panasqueira (tin-) tungsten deposit (Portugal) became completely opaque prior to final homogenization of
236 aqueous two-phase fluid. The infrared device used for this study was designed for near-infrared observation
237 in the spectral range λ = 0.8 to 1.2 µm. At room temperature, FT-IR spectra of various wolframite samples
238 exhibit 2 maxima of IR transmittance in the spectral range λ = 0.8 to 2.5 µm (Fig. 11). On heating, the IR
239 absorption edge between 0.8 and 1.2 µm for a wolframite sample from Panasqueira decreases significantly;
240 also the IR absorption edge starting at ca. 1.8 µm (at room temperature) decreases and shifts to higher
241 wavelengths (Fig. 12). Thus the IR absorption edge between 0.8 and 1.2 µm (at room temperature) became
242 too low for the spectral response of the IR device used by Campbell et al. (1988) and the wolframite samples
243 appeared opaque. When using an infrared microscope equipped with a high resolution IR tube camera it is
244 possible to measure homogenization temperatures of fluid inclusions hosted in wolframite samples from
245 Panasqueira and other tungsten deposits directly (Lüders 1996; Lüders et al. 2009; Ni et al. 2014).
246 Shifting of the IR absorption edges of pyrite samples from various occurrences was also observed by Lüders
247 and Ziemann (1999), Kouzmanov et al. (2002) and Lindaas et al. (2002). For example, Lüders and Ziemann
248 (1999) performed FT-IR measurements on a pyrite sample from the Murgul massive sulfide deposit (Turkey)
249 at 20°C and 100°C and observed that even within this small temperature interval the absorption edge shifted

250 by 0.06 µm to higher wavelengths due to reduction of the band gap energy from 0.91 to 0.87 mV. However,
251 the IR transmittance remained nearly constant even for higher wavelengths. Lindaas et al. (2002) studying IR
252 absorption spectra in the temperature range from room temperature up to 350°C found similar results: a
253 studied pyrite sample from Casapalca, Peru showed an IR absorption edge at ca. 1.3 µm at room temperature
254 that got shifted to ca. 1.7 µm upon heating to 350°C. Due to the shift of the IR absorption edge to higher
255 wavelengths upon heating most of the pyrite samples studied so far by IR microthermometry became
256 completely opaque prior reaching the homogenization temperatures of the fluid inclusions hosted therein. In
257 order to obtain fluid inclusion homogenization temperatures the cycling technique proposed by Goldstein
258 and Reynolds (1994) was applied. Previous studies on pyrite-hosted fluid inclusions were performed using
259 IR-sensitive tube cameras which allow observation in the near-infrared region between 0.8 and max. 2.3 µm.
260 However, the IR sensitivity of such cameras decreases continuously from ca. 1.2 µm onwards (Fig. 6). This
261 seems to be the reason why the transparency of pyrite gradually decreases with on heating. A new generation
262 of InGaAs IR cameras showing nearly constant high IR sensitivity up to 1.8 µm (Fig. 6) may find a remedy
263 for this problem. Figure 13 shows a sequence of IR photomicrographs of pyrite-hosted fluid inclusions taken
264 at different temperatures upon heating in a Linkam TS 600 heating stage. The sample studied here originates
265 from the massive sulfide deposit at Murgul, Turkey and was previously studied by Lüders and Ziemann
266 (1999). In this study the sample became completely opaque at about 250°C when using a Hamamatsu C-
267 2400 IR tube camera designed for application up to 2.3 µm. In contrast, homogenization temperature of
268 individual inclusions could be measured directly at 306.5 and 319.2°C when using a Hamamatsu InGaAs
269 camera. Although the sharpness of the inclusions diminishes upon further heating to 400°C the inclusions are
270 still visible (Fig. 13).
271
272 In summary, there are a several factors such as impurities, chemical composition, and first of all the shift of
273 the IR absorption edges upon heating that control the IR transmittance of ore minerals. When using simple
274 infrared CCD cameras with low IR spectra ranges (0.8 – 1.1 µm) the applicability of infrared microscopy for
275 fluid inclusion studies in opaque minerals is limited to a few minerals such as stibnite, Fe-rich sphalerite and
276 some sulfosalts (Fig. 3, 4). Furthermore, it must be considered that the IR transparency decreases upon

heating due to shifting of the IR absorption edge to higher wavelengths. Fluid inclusions hosted in e.g. pyrite can only be studied when using high-resolution IR tube cameras or InGaAs cameras.

Discussion

Near infrared microscopy applied to studies of fluid inclusions hosted in some opaque ore minerals is a powerful tool for obtaining direct information about the composition and temperature of ore-forming fluids. The method can be applied to common ore minerals such as sphalerite, sulfosalts, pyrite and oxides although it has to be pointed out that there are limiting factors (see previous sections). Fluid inclusion data obtained from ore minerals can be compared with data derived from fluid inclusions hosted in transparent gangue minerals which are associated or intergrown with ore minerals. Only such a comparison allows a statement whether or not ore and gangue minerals precipitated co-genetically from the same fluid. The latter assumption is generally made when studying fluid inclusions are solely measured in e.g. quartz from different types of ore deposits. In cases where fluid inclusion data being derived from ore minerals differ from those of fluid inclusions hosted in transparent gangue minerals the reason for this may be various. Gangue minerals such as quartz or carbonates may easily recrystallize and fluid inclusions may be modified. In contrast, ore minerals such as pyrite have completely different mechanical properties and fluid inclusions therein may preserve the original ore-forming fluid. Dilution of magmatic fluids by meteoric water may be the reason for different homogenization temperatures and salinity of fluid inclusions in ore and gangue minerals in some magmatic epithermal systems (e.g. Mancano and Campbell 1995). Fluctuations in pressure due to fault zone movements may cause adiabatic cooling or decomposition of an ore-forming fluid resulting in a shift of the latter to lower temperatures (Hagemann and Lüders 2003). In sediment-hosted hydrothermal ore deposits fluid mixing is a common mechanism to precipitate ore or gangue minerals.However, under best circumstances, combined studies of fluid inclusions hosted in ore and gangue minerals may indicate such processes and help to decipher the fluid evolution in ore deposits.

Besides a comparison of microthermometric data of fluid inclusions hosted in ore and gangue minerals, fluid inclusions in opaque ore minerals can directly be analyzed for chemical compositions using LA-ICP-MS (Kouzmanov et al. 2010). For fluid inclusions hosted in transparent minerals such as quartz this method is

widely applied using transmitted light microscopy. Kouzmanov et al. (2010) performed detailed mapping of enargite and pyrite samples in infrared transmitted and transmitted-reflected light as well under visible reflected light in order to localize fluid inclusions in the ore minerals prior to laser ablation. No infrared camera was used on the LA-ICP-MS. The study revealed that quartz and pyrite from the Rosia Poieni porphyry copper deposit (Romania) precipitated from chemically distinct hydrothermal fluids (Kouzmanov et al. 2010).

The mapping method used applied by Kouzmanov et al. (2010), however, is highly extensive and could be simplified by some modifications of the LA-ICP-MS. One method to simplify LA-ICP-MS measurements of fluid inclusions hosted in IR-transparent ore minerals would be the replacement of the normal lamp house by an IR lamp house. Transmitted light microscopes are equipped with an IR filter in the pathway of the light. This filter can be removed and be replaced by an IR module, which allows IR light to pass through the microscope. Furthermore, the CCD camera of the LA-ICP-MS must be replaced by an infrared camera. A high-resolution camera is required for good imaging. For better localization of fluid inclusions prior to ablation via the Schwarzschild objective, an IR objective can be used optionally. Fig. 14 shows fluid inclusions hosted in pyrite (see Fig. 13) seen under the Schwarzschild objective of a LA-ICP-MS system modified for IR application. When taking the described modifications into account, LA-ICP-MS analyses of fluid inclusions hosted in some opaque ore minerals can be performed routinely without extensive mapping.

Infrared microscopy also provides a means for directly linking petrological information with age data. Some ore minerals e.g. hematite (e.g. Wernicke and Lippolt 1994, Lüders at al. 2005; Ault et al. 2015), sphalerite (e.g. Nakai et al. 1993; Pettke and Diamond 2000; Morelli et al. 2004), wolframite (Romer and Lüders 2006; Bai et al. 2013) can be dated directly using different age dating techniques. All these minerals show good infrared transmittance and thus the temporal *P-V-T-X* constraints of ore-forming fluids can be derived from fluid inclusions studies and be combined with ages of the ore minerals. In the near future further progress in developing methods for direct dating of ore minerals can be expected. Possibly more IR transparent ore minerals that contain fluid inclusions will become accessible for combined geochronological and fluid inclusion studies.

Conclusions

So far, fluid inclusions hosted in ore minerals in visible light only can be performed in Fe-poor sphalerite and cassiterite as well as in some Ag sulfosalts. Although there are limiting factors, near-infrared light microscopy provides a means of studying fluid inclusions hosted in some common ore minerals that are opaque in visible light. The data obtained from fluid inclusions in ore minerals provide direct information about salinity and temperature of ore-forming fluids. Comparison of microthermometric data obtained from studies of fluid inclusions in ore and gangue minerals may prove genetic relationships of the mineral-forming fluids, e.g. co-precipitation of ore and gangue minerals from a single, fluid mixing. When using IR light microscopy it will be possible to study the chemical composition of fluid inclusions hosted in some opaque ore minerals directly by LA-ICP-MS.

Acknowledgements I am indebted to the curators of the Naturkundemuseum Berlin, G. Wappler and R.-T. Schmitt for providing ore mineral samples used for FT-IR spectroscopy and microprobe analysis in this study. I am grateful to D. Rhede and M. Koch-Müller both GFZ Potsdam for microprobe analysis and FT-IR spectroscopy, respectively. P. Möller is thanked for fruitful discussions on semiconducting properties of ore minerals. The attentive reviews and by Alfons van den Kerkhof and Matthew Steele-MacInnis are gratefully acknowledged.

References

Ault AK, Reiners PW, Evans JP Thompson SN (2015) Linking hematite (U/Th)/He dating with the microtextural record of seismicity in the Wasatch fault damage zone, Utah, USA. Geology 43:771-774.

Bai X-J, Wang M, Jiang Y-D, Qiu H-N (2013) Direct dating of tin–tungsten mineralization of the Piaotang tungsten deposit, South China, by $^{40}Ar/^{39}Ar$ progressive crushing. Geochim Cosmochim Acta 114:1-12

359 Bailly L, Bouchot V, Beny C, Milesi J-P (2000) Fluid inclusion study in stibnite using infrared microscopy:
360 Example of the Brouzils antimony deposit (Vendée, Armorican Massif, France). Econ Geol 95:221-
361 226
362 Behr HJ, Horn EE, Frentzel-Beyme K, Reutel C (1987) Fluid inclusion characteristics of the Variscan and
363 post-Variscan mineralizing fluids in the Federal Republic of Germany. Chem Geol 61:273-285
364 Boldish SI, White WB (1998) Optical band gaps of selected ternary sulfide minerals. Am Mineral 83:865-
365 871
366 Bodnar RJ, Lecumberri-Sanchez P, Moncada D, Steele-MacInnis M (2014) Fluid inclusions in hydrothermal
367 or deposits. In: Holland HD, Turekian KK (eds) Treatise on Geochemistry, 2nd ed Vol 13, Elsevier,
368 Oxford pp:119-142
369 Campbell AR, Robinson-Cook S, Amindyas C (1988) Observation of fluid inclusions in wolframite from
370 Panasqueira, Portugal. Bull Mineral 111:251-256
371 Campbell AR, Panter KS (1990): Comparison of fluid inclusions in coexisting (cogenetic ?) wolframite,
372 cassiterite and quartz from St. Michel´s Mount and Cligga Head, Cornwall, England. Geochim
373 Cosmochim Acta 54:673-681.
374 Campbell AR, Robinson-Cook S (1987): Infrared fluid inclusion microthermometry on coexisting
375 wolframite and quartz. Econ Geol 82:1640-1645.
376 Campbell AR (1991) Geologic applications of infrared microscopy. Soc Sediment Geol, SEPM Short Course
377 25:161-171.
378 Efstathiou A, Levin ER (1968) Optical properties of As_2Se_3, $(As_xSb_{1-x})_2Se_3$ and Sb_2S_3. J Optic Soc Am
379 58:373-377
380 Favorov VA, Krasnikov VI, Sychugov VS (1972) Nekotorje faktory, opredelyayusshchie izmenchivost‘
381 oluprovodnikovykh svoistv pirita i arsenopirita. Izvestiya Akad Nauk SSSR, Seria Geol 11:72-84
382 Fischer M, Hiller JE (1956) Über den thermoelektrischen Effekt des Pyrits. Neues Jb Mineral 89:281-301
383 Fleischer M (1955) Minor elements in some sulfide minerals. Econ Geol 50:970-1024
384 Hagemann SG, Lüders V (2003) P-T-X conditions of hydrothermal fluids and precipitation mechanism of
385 stibnite-gold mineralization at the Wiluna lode-gold deposits, Western Australia: Conventional and
386 infrared microthermometric constraints: Mineral Deposita 38:936–952.

Hawley JE (1952) Spectrographic studies of some Eastern Canada gold mines. Econ Geol 47:778-803

Goldstein RH, Reynolds TJ (1994) Systematics of fluid inclusions in diagenetic minerals. SEPM Short Course 31, 199 p, Tulsa

Hunt GR, Salisbury JW, Lenhoff CJ (1971a) Visible and near-infrared spectra of minerals and Rocks: III. Oxides and hydroxides. Modern Geol 2:195-205

Hunt GR, Salisbury JW, Lenhoff CJ (1971b) Visible and near-infrared spectra of minerals and Rocks: IV. Sulphides and Sulfates. Modern Geol 3:1-14

Karasev AP, Krasnikov VI, Pantaev VD, Seifullin RS, Sychugov VS, Favorov VA (1972) Nekotorje elektrofizicheskie svoistva pirita vostochnogo zabaikalia. Akad Nauk SSSR, Sibirskoe Otdelenie, Geol. i Geofiz 5:64-71

Keys JD, Horwood GL, Baleshta TM, Cabri LJ, Harris DC (1968) Iron-iron interaction in iron-containing zinc sulfide. Canad Mineral 9:463-467

Kouzmanov K, Pettke T, Heinrich CA (2010) Direct analysis of ore-precipitating fluids: Combined IR microscopy and LA-ICP-MS study of fluid inclusions in opaque ore minerals. Econ Geol 105:351-373

Kouzmanov K, Bailly L, Ramboz C, Rouer O, Bény J-M (2002) Morphology, origin and infrared microthermometry of fluid inclusions in pyrite from the Radka epithermal copper deposit, Srednogorie zone, Bulgaria. Mineral Deposita 37:599-613

Kulis J (1999) Trace element control on near-infrared transparency of pyrite. Unpub MS thesis, Socorro, New Mexico Inst Mining Tech, 271 p

Lindaas SE, Kulis J, Campbell AR (2002) Near-infrared observation and microthermometry of pyrite-hosted fluid inclusions. Econ Geol 97:603-618

Lüders V, Romer RL, Gilg HA, Bodnar RJ, Pettke T, Misantoni D (2009) A geochemical study of the Sweet Home Mine, Colorado Mineral Belt, USA: hydrothermal fluid evolution above a hypothesized granite cupola. Mineral Deposita 44:415-434

Lüders V, Romer RL, Cabral AR, Schmidt C, Banks DA, Schneider J (2005) Genesis of itabirite hosted Au–Pd–Pt-bearing hematite-(quartz) veins, Quadrilátero Ferrífero, Minas Gerais, Brazil: constraints from

fluid inclusion infrared microthermometry, bulk crush-leach analysis and U–Pb systematics. Mineral Deposita 40:289-306

Lüders V, Gutzmer J, Beukes JB (1999) Fluid inclusion studies in co-genetic hematite, hausmannite and gangue minerals from high-grade manganese ores in the Kalahari manganese filed, South Africa. Econ Geol 94:589-596

Lüders V, Ziemann M (1999) Possibilities and limits of infrared light microthermometry applied to studies of pyrite-hosted fluid inclusions. Chem Geol 154:169-178.

Lüders V (1996) Contribution of infrared microscopy to fluid inclusion studies in some opaque minerals (wolframite, stibnite, bournonite); metallogenic implications. Econ Geol 91:1462-1468

Mancano DP, Campbell AR (1995): Microthermometry of enargite-hosted fluid inclusions from Lepanto, Philippines, high-sulfidation Cu-Au deposit. Geochim Cosmochim Acta 59:3909-3916.

Moncada D, Mutchler S, Rimstidt JD, Reynolds TJ, Bodnar RJ (2012) Characteristics and distribution of mineral textures and fluid inclusions in the epithermal Ag-Au deposits at Guanajuato, México. J Geochem Explor 114:20-35

Morelli RM, Creaser RA, Selby D, Kelley KD, Leach DL, King AR (2004) Re–Os sulfide geochronology of the red dog sediment-hosted Zn–Pb–Ag deposit, Brooks Range, Alaska. Econ Geol 99:1569–1576

Moritz R (2006) Fluid salinities obtained by infrared microthermometry of opaque minerals: Implications for ore deposit modeling - A note of caution. J Geochem Explor 89:284-287

Nakai S, Halliday AN, Kessler SE, Jones HD, Kyle JR, Lanes TE (1993) Rb-Sr dating of sphalerites from Mississippi Valley-type (MVT) ore deposits. Geochim Cosmochim Acta 57:417-427

Ni P, Wang X-D, Wang G-G, Huang J-B, Pan J-Y, Wang T-G (2005) An infrared microthermometric study of fluid inclusions in coexisting quartz and wolframite from Late Mesozoic tungsten deposits in the Gannan metallogenic belt, South China. Ore Geol Rev 65:1062-1077

Pettke T, Diamond LW (1996) Rb-Sr dating of sphalerite based on fluid inclusion - host mineral isochrons: a clarification of why it works. Econ Geol 91:951-956

Pflugbeil B (1995) Mikrothermometrische Untersuchungen an Flüssigkeitseinschlüssen in Wolframiten aus Quarz-Wolframit-Mineralisationen mittels IR-Mikroskopie. Unpub Dipl thesis, Tech Univ Berlin, 59 p

Richards JP, Kerrich R (1993) Observations of zoning and fluid inclusions in pyrite using a transmitted infrared light microscope. Econ Geol 88:716-723

Roedder E, Bodnar RJ (1997) Fluid Inclusion Studies of Hydrothermal Ore Deposits. In: Barnes HL (ed) Geochemistry of Hydrothermal Ore Deposits, 3rd ed., Wiley & Sons, New York, pp 657-697

Romer RL, Lüders V (2006) Direct dating of hydrothermal W mineralization: U-Pb age for hübnerite ($MnWO_4$), Sweet Home Mine, Colorado. Geochim Cosmochim Acta 70:4725-4733

Rosière CA, Rios JR (2004) The origin of hematite in high-grade iron ores based on infrared microscopy and fluid inclusion studies: the example of the Conceição mine, Quadrilátero Ferrífero, Brazil. Econ Geol 99:611-624

Schoolar RB, Dixon JR (1965) Optical constants of lead sulfide in the fundamental adsorption edge region. Phys Rev 137:A667-A670

Seehra MS, Seehra SS (1979) Temperature dependence of the band gap of FeS_2. Phys Rev B19:6620

Shuey RT (1975) Semiconducting ore minerals. Developments in Econ Geol 4, 415 p, Elsevier, Amsterdam, Oxford, New York

Shimizu T, Masahiro A (2003) Near-infrared and visible light microthermometry of fluid inclusions in sphalerite from a possible southeast extension of the Toyoha polymetallic deposit, Japan. Resource Geol 53:115-126

Telkes M (1950) Thermoelectric power and electrical resistivity of minerals. Amer Mineral 35:536-555

Tindle AG, Webb PC (1989) Niobian wolframite from Glen Gairn in the Eastern Highlands of Scotland: A microprobe investigation. Geochim Cosmochim Acta 53:1921-1935

Wernick JH, Benson KE (1957) New semiconducting ternary compounds. J Phys Chem Solids 3:157-159

Wernicke RS, Lippolt HJ (1994) Dating of vein specularite using internal $(U+Th)/^4He$ isochrons. Geophys Res Lett 21:345-347

Wilkinson JJ (2001) Fluid inclusions in hydrothermal ore deposits. Lithos 55:229-272

Woods TL, Roedder E, Bethke PM (1982) Fluid-inclusion data on samples from Creede, Colorado, in relation to mineral paragenesis. USGS open-file report 82-313, 77 pp

Zhu M-T, Zhang L-C, Wu G, He H-Y, Cui M-L (2003) Fluid inclusions and He-Ar isotopes in pyrite from the Yinjiagou deposit in the southern margin of the North China Craton: A mantle connection for poly-metallic mineralization. Chem Geol 351:1-14

Figure captions

Fig. 1: Energy band models different types of semi-conductors. A) Intrinsic semiconductors have the same number of electrons and holes. The radiation energy needed to excite electrons to move from the valence band to the conduction band is called „band gap energy“ (Eg). B and C) Impurity semiconductors (e.g. many ore minerals) have either a surplus (n-type) or shortfall (p-type) in valence electrons and thus the conductivity of both types of semiconductors is enhanced compared to that of intrinsic semiconductors (for details see text).

Fig. 2: Fournier transmission infrared (FT-IR) spectra of galena thick sections (90 µm) from Neudorf, Harz Mts. (Germany), Freiberg, Saxony (Germany), Durham, North Pennine Orefield (U.K.) obtained using a Bruker Vertex 80v spectrometer. The infrared absorption edges of the studied samples show different quality of IR transmittance above 3 µm. Since the IR sensitivity of available IR cameras is only limited to observation in the near infrared region up to ca. 2.3 µm fluid inclusions hosted in galena cannot be studied, i.e., galena samples are opaque in the spectral range of any microscope IR camera.

Fig. 3: FT-IR spectra of stibnite, enargite and bournonite thick sections (90 µm) from different occurrences (Wiluna, Western Australia; Emerli, Turkey; Chelopech, Bulgaria; Clausthal, Harz Mts., Germany). Both FT-IR spectra of stibnite show slightly increasing IR transmission with increasing wavelength but different quality of IR transmission probably due to trace element content (for details see text). The FT-IR spectra of enargite and bournonite increase from 0.9 to about 1.2 µm and show more or less constant IR transmittance in the detected spectral range.

Fig. 4: FT-IR spectra of sphalerite thick sections (90 µm) from different occurrences (Neudorf/Harz Mts., Germany; Lavrion, Greece; Freiberg/Saxony, Germany; Pirquitas, Argentina; Vent field, North Fiji Basin; Zinnwald/Saxony, Germany). All Fe-rich samples as well as wurtzites (Pirquitas, North Fiji Basin) are not transparent for visible light but show transmittance in the near infrared region.

Fig. 5: FT-IR spectra of tetrahedrite-tennantite thick sections (90 µm) showing different quality of IR transmittance with increasing As-content (see also Table 1).

Fig. 6: Sensitivity curves of different IR cameras. Some CCD cameras are sensitive for observations in the very near infrared region up to ca. 1.2 µm. Cameras with IR sensitive tubes are sensitive to wavelengths up to 2.3 µm but show decreasing sensitivity curves that are considerably lower in the spectral range λ = 1 to 1.8 µm compared to those of InGaAs IR cameras. The latter show more or less constant sensitivity up to 1.8 µm.

Fig. 7: Infrared photomicrograph of wolframite-hosted fluid inclusions from Panasqueira, Portugal. Photo was taken using a Q/Cam IR Fast 1394 camera.

Fig. 8) FT-IR spectra of hematite thick sections (90 µm) from different occurences (Rio Marina, Isle Elba, Italy; Itabira, Minas Gerais, Brazil; Wessel´s Mine, Kalahari manganese field, South Africa, Schönberg Mine, Germany). All FT-IR spectra of the studied hematite samples show increasing IR transmittance

524 starting at different wavelengths. Fluid inclusions hosted in hematite samples from Rio Marina and Wessel´s
525 Mine can be observed with IR sensitive CCD cameras whereas other samples can only be studied using IR
526 cameras which higher IR resolution (e.g., IR tube cameras, InGaAs cameras).
527
528 Fig. 9: Infrared microphotograph of pyrite-hosted fluid inclusions from Murgul, Turkey. Photo was taken
529 using a Hamamatsu C-2400 camera with an IR sensitive tube.
530
531 Fig. 10: IR microscope vs. transmitted light microscope microthermometric data of selected samples (data
532 from Pflugbeil 1995).
533
534 Fig. 11: FT-IR spectra of wolframite thick sections (90 μm) from different occurrences (Panasqueira,
535 Portugal; Pechtelsgrün and Sauberg, Saxony, Germany; Lake District, UK; Glen Gairn, Scotland).
536 Wolframite samples showing IR transmittance show 2 IR absorption edges. The quality of IR transmittance
537 of the studied samples is highly variable probably due to variable Fe:Mn ratios (Pflugbeil 1995) or different
538 trace element contents. Wolframite samples from Glen Gairn may contain up to nearly 8 wt. % Nb_2O_5
539 (Tindle and Webb 1989) are opaque for IR light.
540
541 Fig. 12: FT-IR spectra of a wolframite thick section (90 μm) from Panasqueira, Portugal obtained at different
542 temperatures using a Linkam TS 600 heating stage. For details see text.
543
544 Fig. 13: Observation of phase transitions of pyrite-hosted aqueous two-phase fluid inclusions during heating
545 runs using an Olympus BHSM-IR microscope equipped with a Linkham TS 600 heating stage and an
546 InGaAs IR camera (spectral range λ = 0.8 to 1.8 μm). Phase relations of the inclusions at room temperature
547 are shown in Fig. 9.
548 In the temperature range between 175 and 275°C the bubbles in both inclusions become continuously
549 smaller. Note the clarity of the inclusions does not get diminished significantly when using an InGaAs IR
550 camera. In contrast, the same samples got opaque at ca. 250°C when using a high-resolution IR tube camera
551 (Lüders and Ziemann 1999). At 306.6 °C the bubble in the smaller inclusion homogenizes. Homogenization

552 of the bubble in the bigger inclusions occurs at 319.2°C. Upon further heating to 400°C the big inclusion
553 decrepitates at 378.3°C. At 400°C the image gets diminished but the inclusions are still visible.
554
555 Fig. 14: Photomicrograph of pyrite-hosted fluid inclusions also shown in Fig. 9 and 13. The photo was taken
556 using a Schwarzschild objective of LA-ICPMS system modified for IR applications. For details see text.
557 Note that the photo was taken after performing heating runs shown in Fig. 13 and that the big inclusions to
558 the right decrepitated at 378.3°C.
559

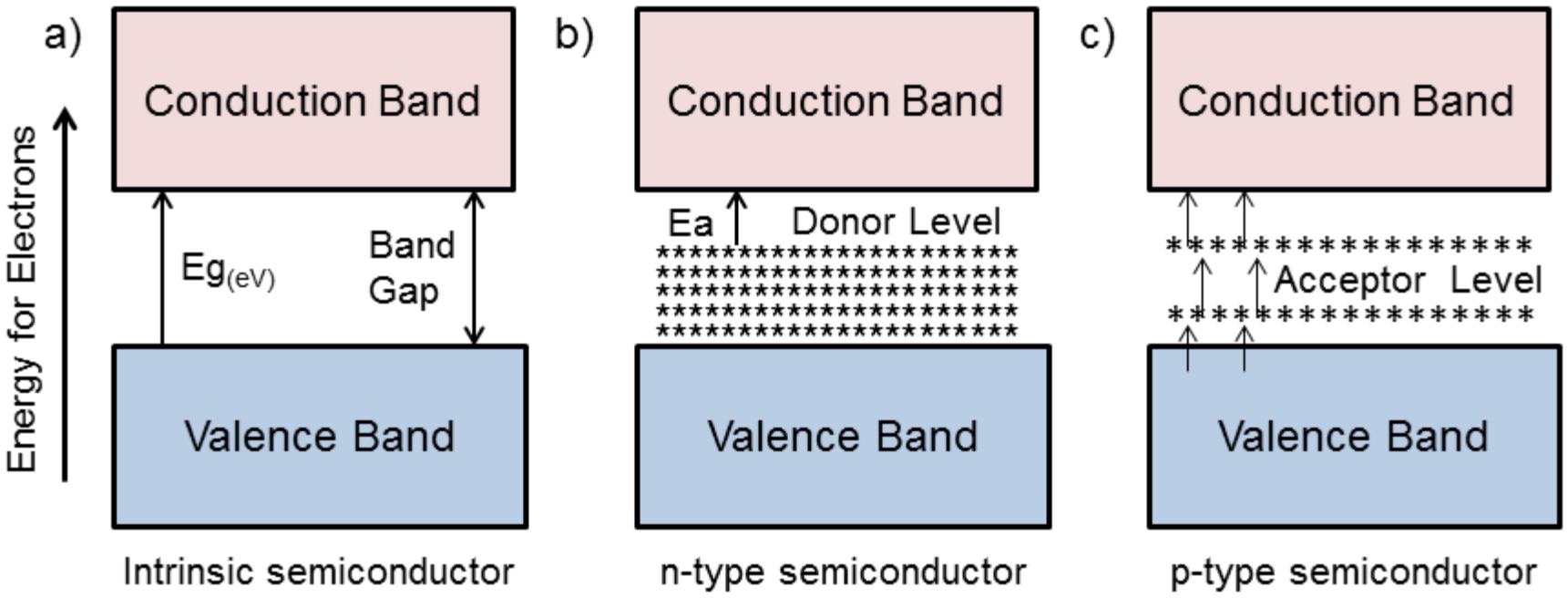
a)
Conduction Band
Energy for Electrons
Eg(eV)
Band
Gap
Valence Band
Intrinsic semiconductor
b)
Conduction Band
Ea
Donor Level
Valence Band
n-type semiconductor
c)
Conduction Band
Acceptor Level
Valence Band
p-type semiconductor

Fig. 1.

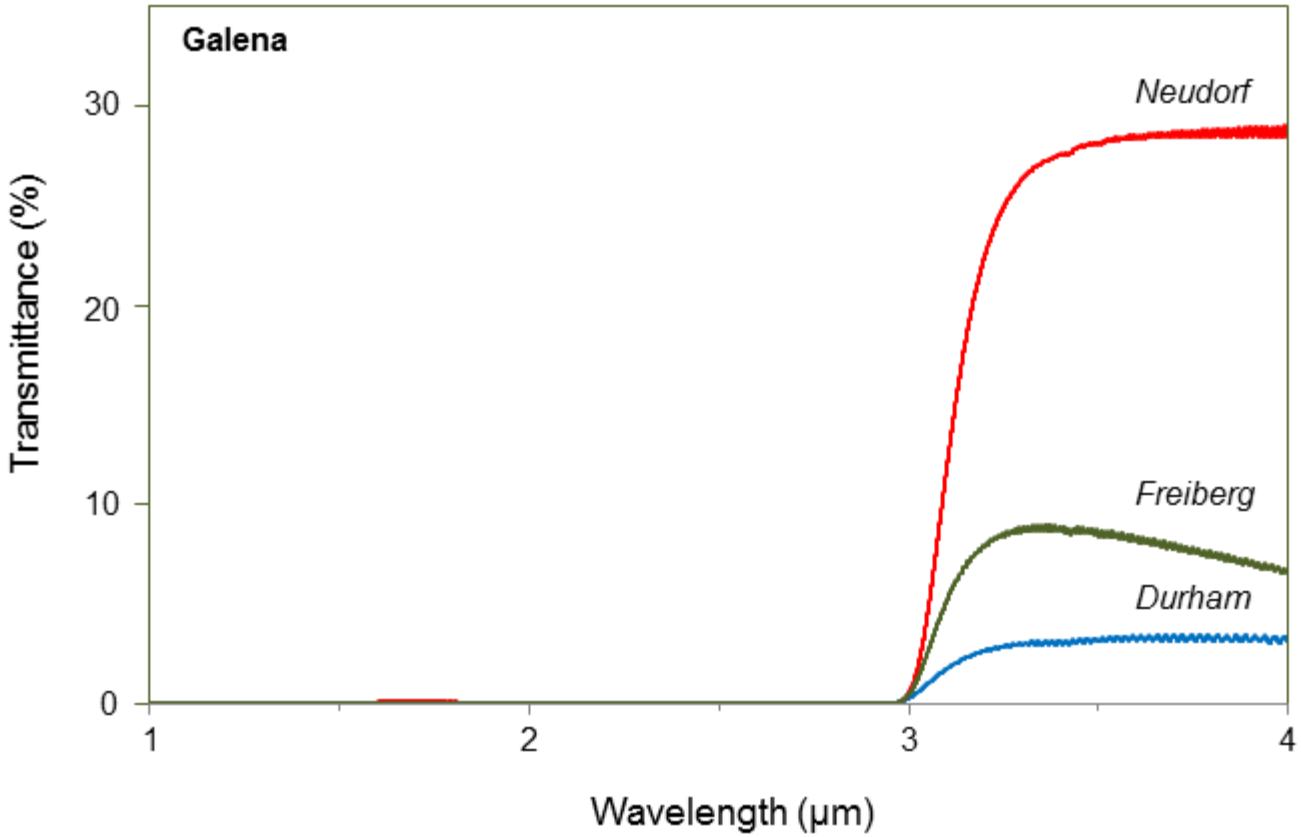
Galena
Neudorf
Freiberg
Durham
Transmittance (%)
0
10
20
30
1
2
3
4
Wavelength (µm)

Fig. 2

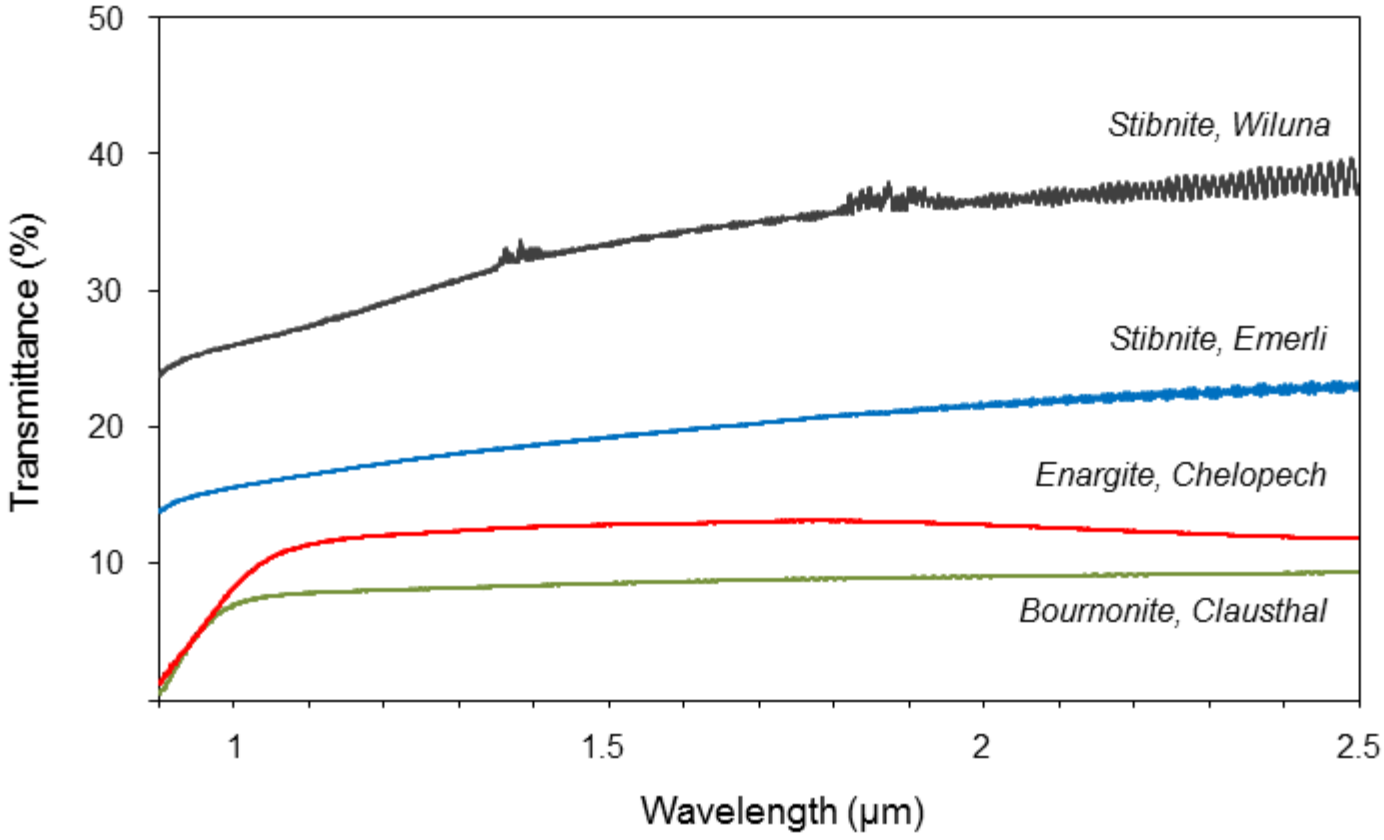
50
40
30
20
10
Transmittance (%)
Stibnite, Wiluna
Stibnite, Emerli
Enargite, Chelopech
Bournonite, Clausthal
1
1.5
2
2.5
Wavelength (μm)

Fig. 3

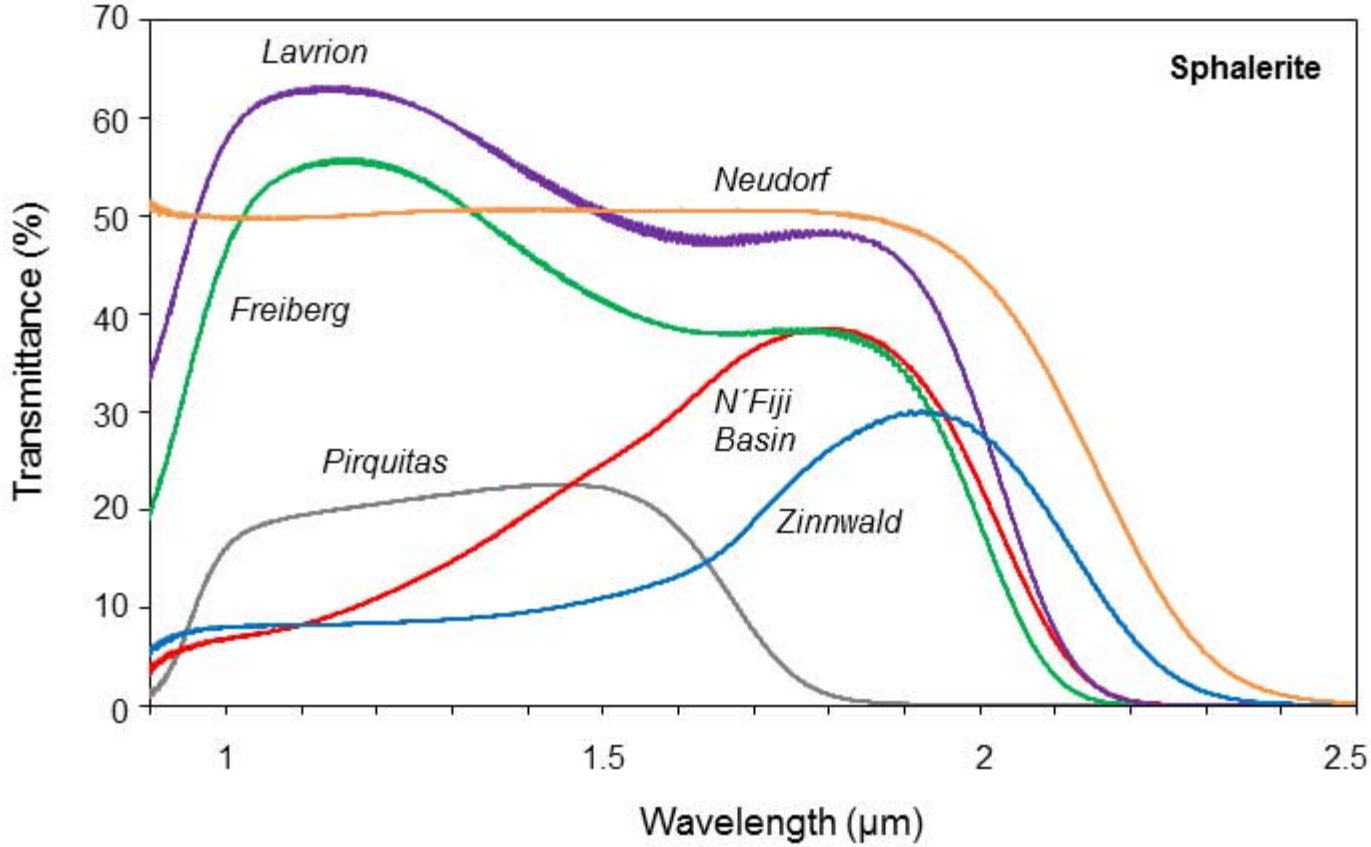
Sphalerite
Lavrion
Neudorf
Freiberg
N´Fiji
Basin
Pirquitas
Zinnwald
Transmittance (%)
Wavelength (µm)
70
60
50
40
30
20
10
0
1
1.5
2
2.5

Fig. 4

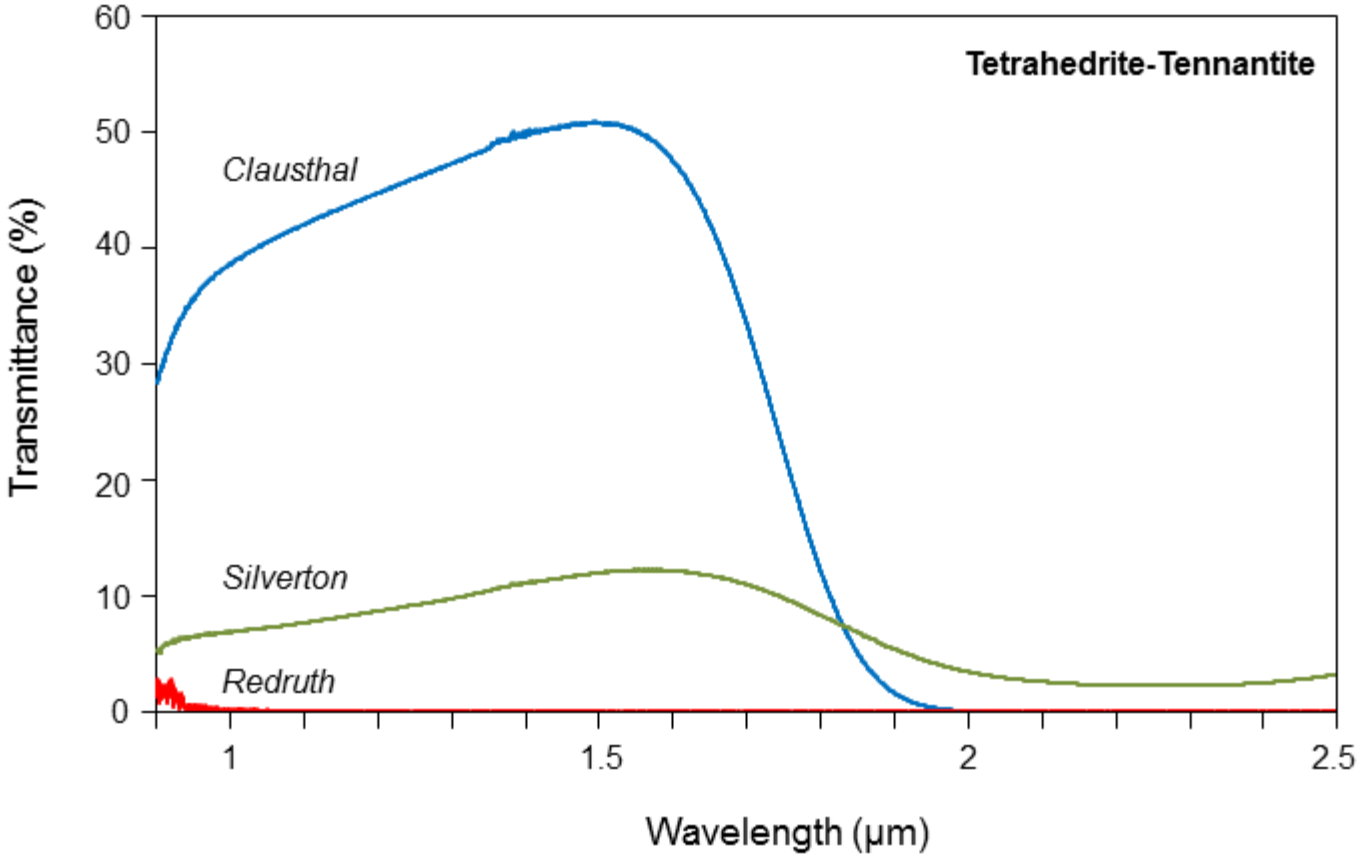
Tetrahedrite-Tennantite
Clausthal
Silverton
Redruth
Transmittance (%)
60
50
40
30
20
10
0
1
1.5
2
2.5
Wavelength (µm)

Fig. 5

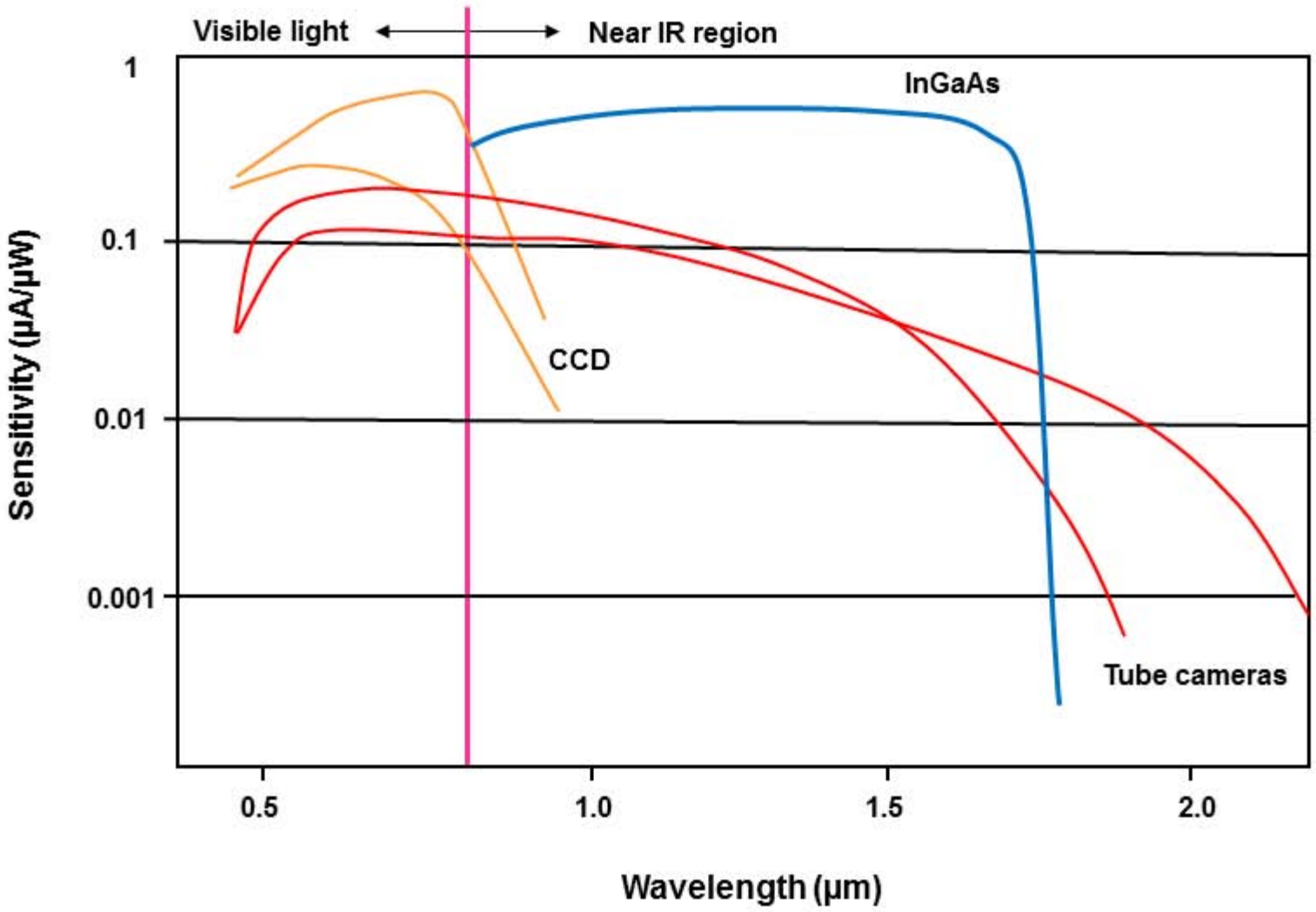
Visible light
Near IR region
1
0.1
0.01
0.001
Sensitivity (μA/μW)
InGaAs
CCD
Tube cameras
0.5
1.0
1.5
2.0
Wavelength (μm)

Fig. 6

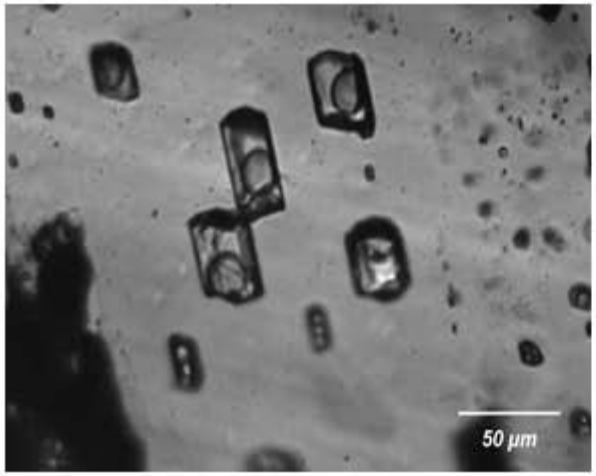

Fig.7

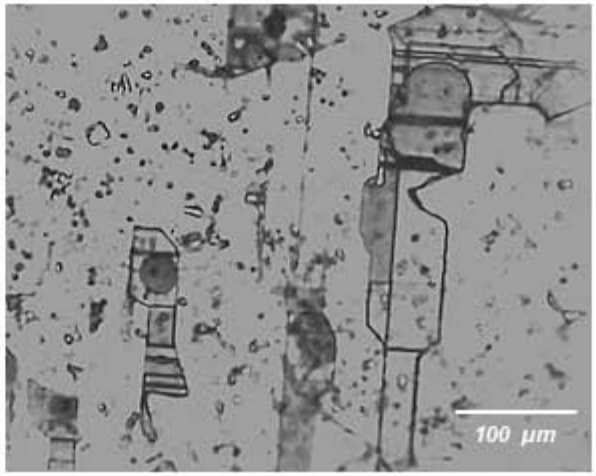

Fig.9

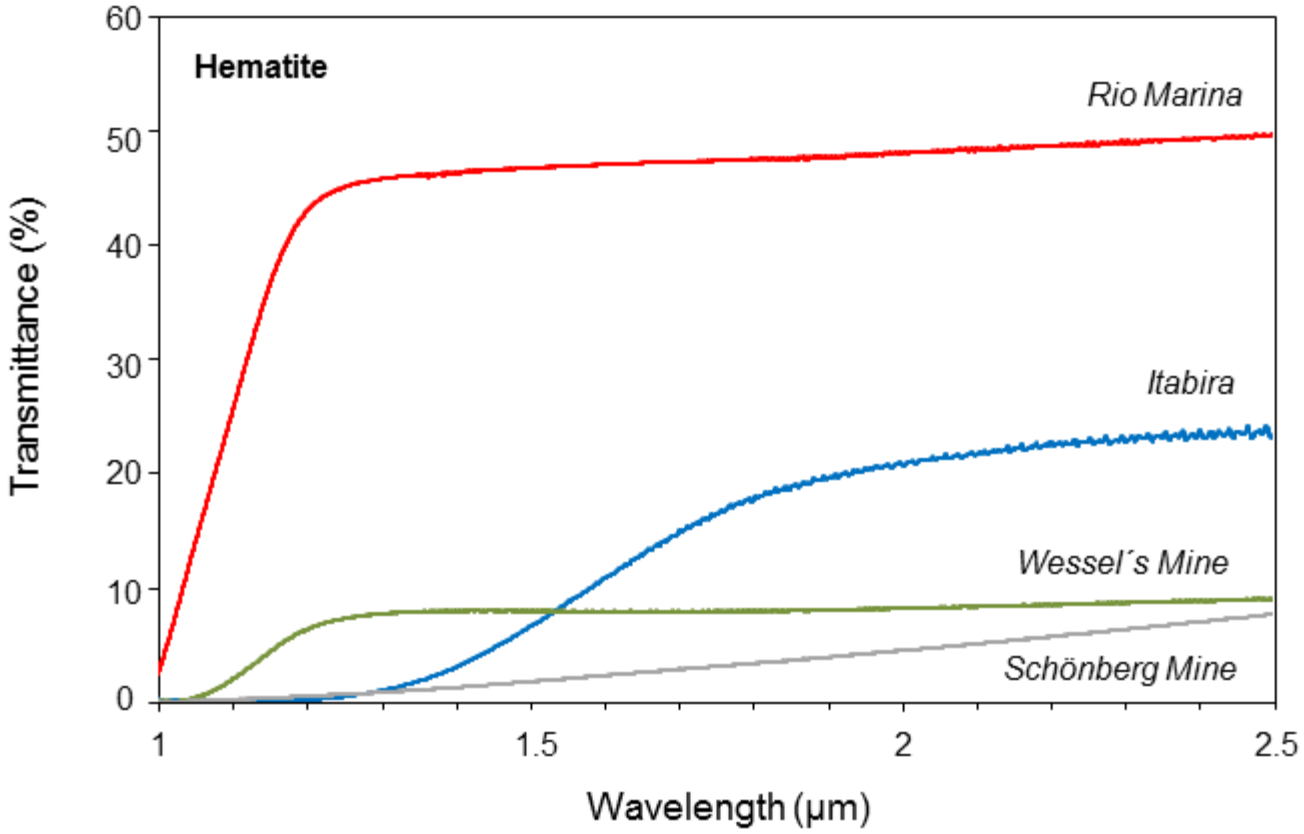
Hematite
Rio Marina
Itabira
Wessel´s Mine
Schönberg Mine
Transmittance (%)
Wavelength (µm)
60
50
40
30
20
10
0
1
1.5
2
2.5

Fig. 8

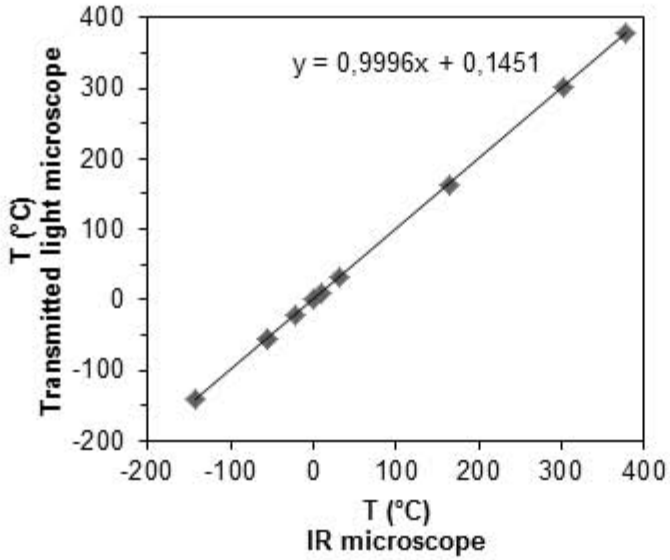
y = 0,9996x + 0,1451
T (°C)
Transmitted light microscope
T (°C)
IR microscope
400
300
200
100
0
-100
-200
-200
-100
0
100
200
300
400

Fig. 10

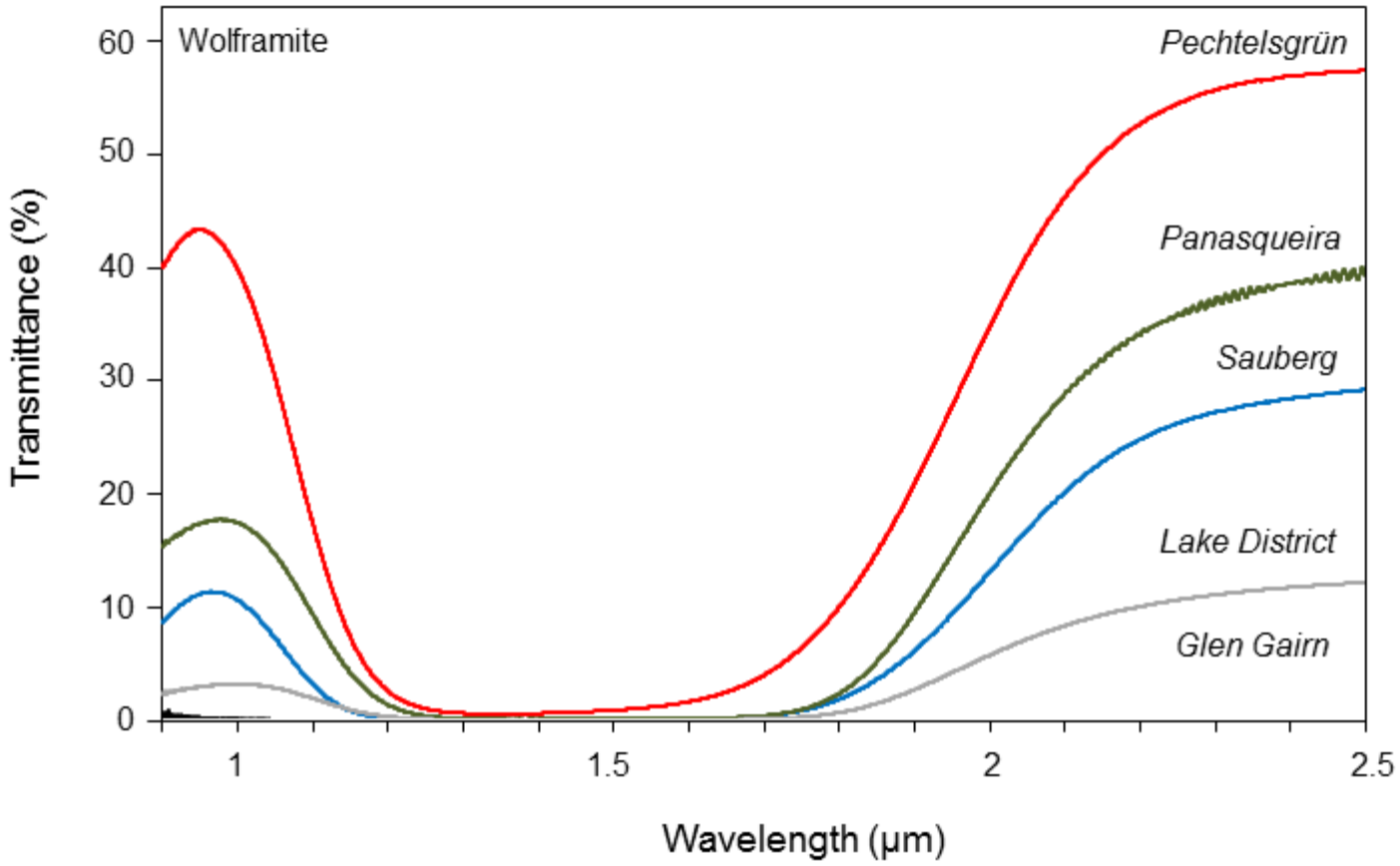
Wolframite
Pechtelsgrün
Panasqueira
Sauberg
Lake District
Glen Gairn
Transmittance (%)
Wavelength (µm)
0
10
20
30
40
50
60
1
1.5
2
2.5

Fig.11

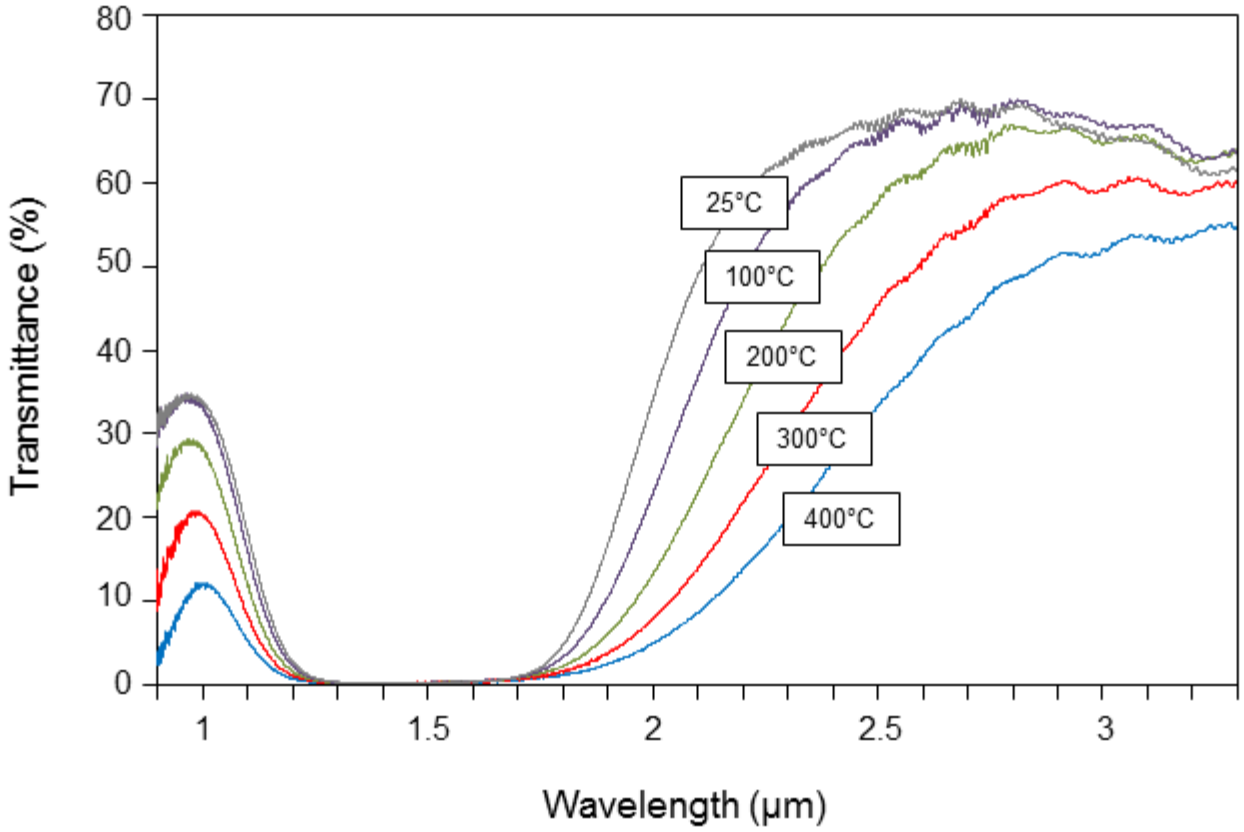
Transmittance (%)
80
70
60
50
40
30
20
10
0
1
1.5
2
2.5
3
Wavelength (μm)
25°C
100°C
200°C
300°C
400°C

Fig.12

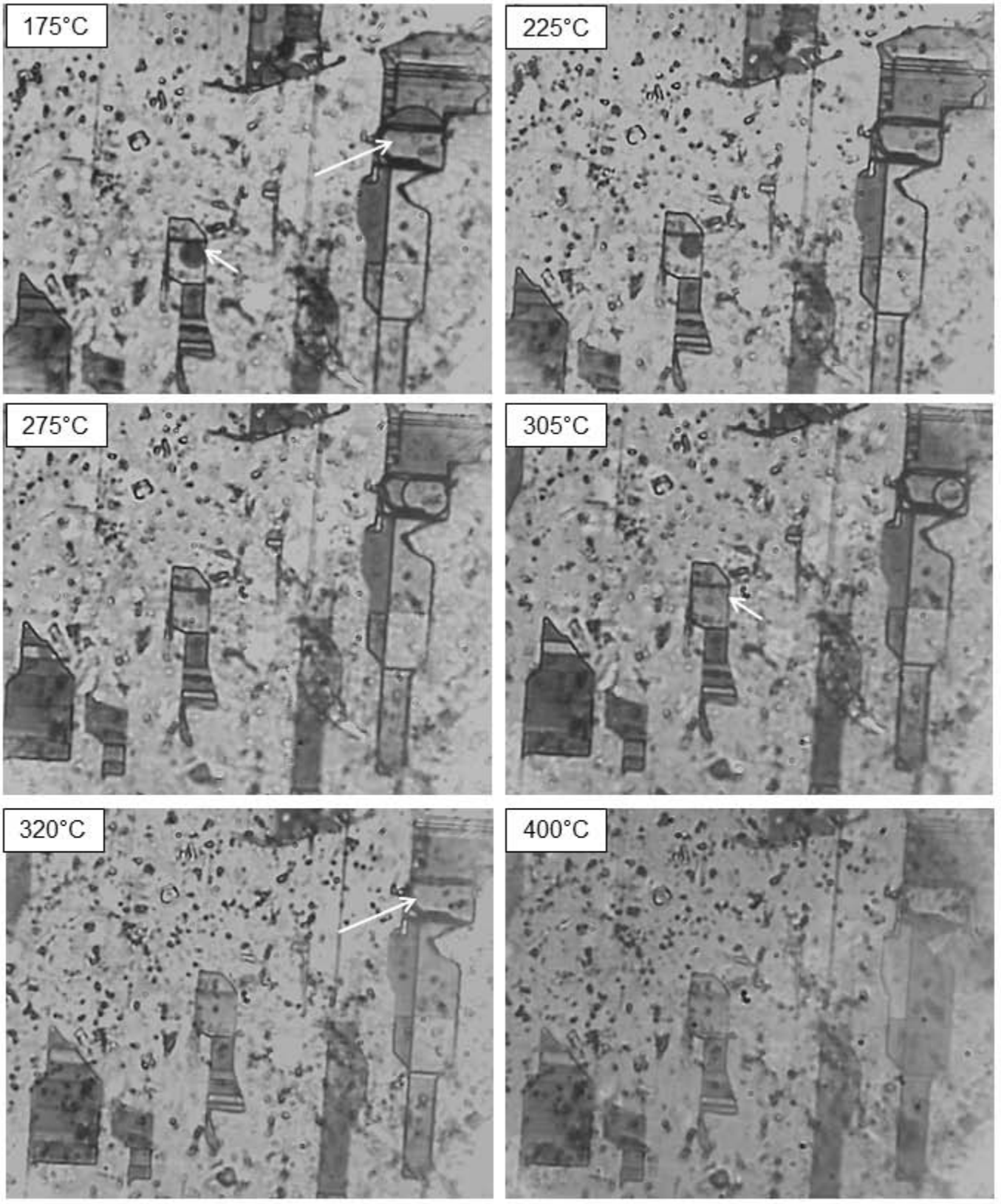
175°C
225°C
275°C
305°C
320°C
400°C

Table 1 Optical observations of tetrahedrite-tennantite samples in the near infrared region (λ = 0.8 – 2.3 µm).

Sample	**1**	**2**	**3**	**4**	**5**	**6**	**7**	**8**	**9**	**10**	**11**	**12**	**13**
wt. %													
S	24.69	24.9	23.61	25.32	24.69	25.4	27.13	25.79	21.42	27.63	28.07	28.16	28.01
Cu	36.66	36.7	30.62	37.51	35.42	38.72	40.38	39,88	32.24	41.5	41.62	43.1	43.48
Sb	27.9	27.73	28.49	24.33	25.12	22.26	9.69	19.8	24.79	3.69	0.3	0.8	0.4
As	1.96	2.09	0.88	4.31	3.41	5.3	14.2	6.56	0.38	17.85	20.26	20.13	19.76
Fe	1.87	2.63	1.46	0.5	3.68	4.25	3.33	4.09	0.56	5.14	2.12	0.3	1.52
Co	0	0	0	0	0	0	0	0	0	0	0	0	0
Zn	5.52	4.64	5.99	7.3	3.15	2.56	4.41	0.94	0.51	2.22	6.58	7.77	6.56
Ni	0	0	0	0	0	0	0	0	0	0	0	0	0
Ag	1.38	0	9.1	1.45	3.87	0.2	0.3	0.3	0	0.4	0.4	0	0
Hg	0.1	0	0	0.1	0.58	0.89	0.1	1.95	18.83	0	0.1	0.1	0.1
Bi	0	0	0	0	0	0.86	0	0	0.2	0.3	0	0	0.68
Pb	0	0	0	0	0	0	0	0	0	0	0	0	0
Total	100.08	98.69	100.15	100.82	99.92	100.44	99.99	99.31	98.93	98.73	99.45	100.36	100.51
IR transparency	good	good	good	fair	patchy	patchy	low	opaque	opaque	opaque	opaque	opaque	opaque

Sample localities: 1) Müsen/Sieg (Germany); 2) Clausthal/Harz Mts. (Germany); 3) Huanchaca (Bolivia); 4) Silverton/Colorado (USA); 5) Kamsdorf (Germany); 6) Spania Dolina (Slowakia); 7) Berjosowski (Russia); 8) Quenza (Algeria); Moschel-Landsberg (Germany); 10) Clara Mine/Black Forest (Germany); 11) Freiberg/Saxony (Germany); 12) Tsumeb (Namibia); Redruth/Cornwall (UK)